EasyChair Preprint

№ 3897

Capillary Trapping of CO2 in a Heterogeneous Horizontal Aquifer

Edward Hinton and Andrew Woods

July 18, 2020

22nd Australasian Fluid Mechanics Conference AFMC2020
Brisbane, Australia, 6–10 December 2020
DOI: 10.14264/uql.2020.xxYY

Capillary trapping of CO_2 in a heterogeneous horizontal aquifer

Edward M. Hinton[1], **Andrew W. Woods**[1]

[1] BP Institute, Department of Earth Sciences, University of Cambridge, Cambridge CB3 0EZ, UK

Abstract

We consider the capillary trapping of carbon dioxide in a horizontal aquifer. Motivated by the heterogeneous nature of reservoir rocks, we allow the permeability to vary vertically across the aquifer. The CO_2 spreads under buoyancy following the end of the injection period. We derive a parabolic governing equation for the motion, which accounts for the trapping of CO_2 at the trailing edge. The flow behaves in a self-similar fashion at early times when it is confined and at late times when it is effectively unconfined. We determine how these similarity solutions are influenced by vertical heterogeneity. We quantify the late-time position of the leading edge of the CO_2 and show that it is highly sensitive to the permeability at the top of the aquifer but rather insensitive to the permeability structure elsewhere. Our results have important implications for the volume of CO_2 that may be stored at a particular geological site.

Keywords
carbon dioxide storage; flow in porous media; gravity currents

Introduction

Carbon capture and storage (CCS) is a key tool for reducing anthropogenic CO_2 emissions from industry and power generation in the medium term. The CO_2 is captured, compressed and then injected into an underground geological formation. The viability of CCS projects depends on ensuring that the CO_2 does not migrate out of the formation.

Typically, the geological formations are porous aquifers that may be bounded above and below by impermeable seal layers [3]. It is important to quantify how far and how fast the buoyant injected CO_2 spreads following the end of the injection period [7]. The volume of mobile CO_2 gradually diminishes in time as it slumps and the CO_2 is trapped owing to capillary forces in the pore throats at the receding edge (see figure 1). The CO_2 also dissolves in the ambient brine but the mass loss is much slower than that associated with capillary trapping.

Previous studies have investigated the effect of capillary trapping on the evolution of the current in horizontal aquifers [6, 2, 3]. These researchers have analysed the influence of confinement associated with a lower boundary and considered two-dimensional and axisymmetric geometries on the extent of the CO_2 current. They considered aquifers with constant permeability and Hesse *et al.* [3] suggested that heterogeneities may have a strong effect on the trapping and migration of CO_2.

Many of the reservoir rocks selected for CO_2 storage have vertical variations in permeability owing to their formation from settling turbidity currents. It has been shown that such vertical variations can substantially alter the flow structure and the extent of the CO_2 during the injection phase [4, 5]. In the present paper, we consider the effect of vertical variations in permeability on the post-injection migration in which the capillary trapping of CO_2 plays a dominant role.

We first develop a model for the post-injection migration of the CO_2 current by adapting the approach of Hesse *et al.* [3] to account for vertical permeability variations [4]. We then analyse the early behaviour when the current spans the thickness of the aquifer, quantifying the effect of the heterogeneity. At late times, the CO_2 occupies a thin region near the upper boundary where it accesses only a small part of the permeability variation. The evolution is then similar to that in an aquifer with constant permeability. We determine how the early evolution, which is influenced by heterogeneity, effects the late-time behaviour. Our results suggest that the volume of CO_2 that may be stored in a particular aquifer is determined primarily by the permeability at the top of the aquifer and the structure elsewhere has a smaller influence.

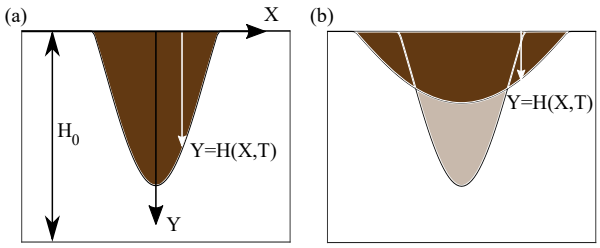

Figure 1. Schematic diagram of the model problem. (a) The instantaneous release of a fixed volume of CO_2 (dark brown). (b) The CO_2 slumps owing to buoyancy and a fraction is capillary trapped in the pore space (light brown). The volume of the mobile CO_2 (dark brown) reduces in time owing to this trapping.

Model

We analyse the post-injection flow of supercritical CO_2 in a horizontal laterally extensive confined aquifer with impermeable boundaries at the top and bottom. The aquifer has thickness H_0. The CO_2 has density ρ and viscosity μ_r, whilst the ambient brine has density $\rho+\Delta\rho$ and viscosity μ_a. The viscosity ratio is

$$m = \mu_r/\mu_a. \tag{1}$$

The horizontal coordinate is denoted by X and the vertical coordinate (measured in the downwards direction) is denoted by Y (see figure 1). We consider aquifers in which the permeability varies in the vertical direction,

$$K = \bar{K}k(Y/H_0) \tag{2}$$

where $k(Y/H_0)$ is the dimensionless permeability defined relative to the mean permeability, $\bar{K} = \frac{1}{H_0}\int_0^{H_0} K(Y/H_0)\mathrm{d}Y$. We define the following depth-integrated permeability [5]

$$\Psi(H/H_0) = \int_0^H k(Y/H_0)\mathrm{d}Y. \tag{3}$$

We assume that the porosity, ϕ, is constant. In addition, we neglect the transition zone between the fluids, which is occupied by varying saturations of both fluids, and we assume that there is a sharp interface between the fluids, with the saturation either side a constant [3]. We denote the thickness of the mobile CO_2 by $Y = H(X,T)$. In CO_2 storage projects, the lengthscale of the

injected current is typically much larger than the aquifer thickness. Thus, the lateral velocity is much larger than the cross-aquifer velocity and the pressure is approximately hydrostatic.

We are interested in analysing the capillary trapping of CO_2 in an aquifer with vertically varying permeability. We focus on the behaviour after injection has ceased. We introduce the following two constant parameters: S_a represents the residual saturation of immobile ambient brine left behind as the CO_2 fluid invades the pore space, whilst S_r represents the residual saturation of the CO_2 left behind when the brine invades the pore space. CO_2 is trapped in the pore spaces as the current slumps and the mobile volume of CO_2 reduces over time (see figure 1). The volume of CO_2 trapped during the injection phase is negligible because there are no regions in which the brine displaces the CO_2.

Since the pressure is hydrostatic, the velocity of the CO_2 in the post-injection phase is given by [3, 4]

$$U = -\frac{\Delta\rho g\bar{K}}{\mu_r}\frac{mk(Y/H_0)(1-\psi(H/H_0))}{m+(1-m)\psi(H/H_0)}\frac{\partial H}{\partial X}. \qquad (4)$$

By applying mass conservation of the CO_2, we obtain the governing equation for the shape of the interface, $Y = H(X,T)$,

$$\frac{\partial H}{\partial T} = \kappa H_0\frac{\partial}{\partial X}\left[\frac{m\psi H/H_0(1-\psi(H/H_0))}{m+(1-m)\psi(H/H_0)}\frac{\partial H}{\partial X}\right]. \qquad (5)$$

where κ is the conductivity of the CO_2, given by the following expression,

$$\kappa = \begin{cases} \kappa_1 = \frac{\Delta\rho g\bar{K}}{\phi(1-S_a-S_r)\mu_r} & \text{for} \quad \partial H/\partial T < 0 \\ \kappa_0 = \frac{\Delta\rho g\bar{K}}{\phi(1-S_a)\mu_r} & \text{for} \quad \partial H/\partial T > 0, \end{cases} \qquad (6)$$

where $\kappa_1 \geq \kappa_0$. The CO_2 is trapped at the receding edges of the current and the volume of mobile CO_2 decreases in time for $\varepsilon > 0$.

We introduce the following scaled properties,

$$h = H/H_0, \qquad x = X/H_0, \qquad t = \kappa_1 T/H_0, \qquad (7)$$

to obtain the dimensionless governing equation for the interface shape, $h(x,t)$,

$$\frac{\partial h}{\partial t} = \sigma\frac{\partial}{\partial x}\left[g(h)\frac{\partial h}{\partial x}\right], \qquad (8)$$

where

$$g(h) = \frac{m\psi(h)[1-\psi(h)]}{m+(1-m)\psi(h)}, \qquad (9)$$

is the flux function and

$$\sigma = \begin{cases} 1 & \text{for} \quad h_t < 0 \\ 1-\varepsilon & \text{for} \quad h_t > 0, \end{cases} \qquad (10)$$

with $\varepsilon = S_r/(1-S_a)$ representing the effect of the capillary trapping of the CO_2 at the receding edge of the current.

The model derived here is applicable to any continuous permeability variation, $k(y)$. Since we are interested in understanding the leading order effect of cross-aquifer permeability variations, we use the following linear profile,

$$k(y) = 1 + \Delta k(y - 1/2), \qquad (11)$$

where $-2 < \Delta k < 2$ is the increase in permeability from the top to the bottom of the aquifer ($\Delta k < 0$ corresponds to a decrease).

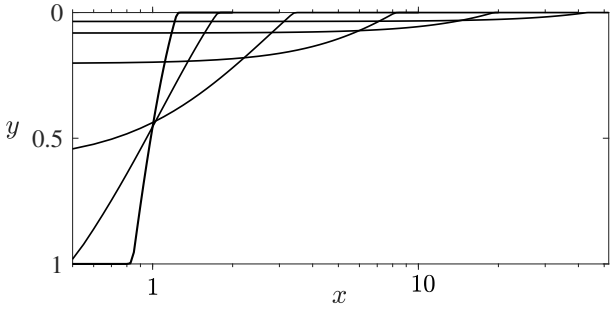

Figure 2. Interface shapes at $t = 0.1, 1, 10, 10^2, 10^3, 10^4$ in an aquifer with constant permeability ($\Delta k = 0$) with no capillary trapping ($\varepsilon = 0$). The viscosity ratio is $m = 0.2$. The interface is symmetric about $x = 0$.

This linear permeability profile allows the effect of a permeability variation to be analysed through a single parameter, Δk, which captures its direction and magnitude.

The post-injection evolution of the current in the case of varying permeability and capillary trapping is complex. Therefore, to focus on the effect of the permeability variation, we restrict our attention to the simple idealized initial condition,

$$h = \begin{cases} 1 & \text{for} \quad -x_0 < x < x_0 \\ 0 & \text{otherwise,} \end{cases} \qquad (12)$$

where x_0 is the aspect ratio of the initial shape. For detailed analysis of the effect of different end of injection current shapes, see [7]. Indeed, it would be straightforward to extend our study to consider other initial conditions.

The initial dimensionless volume of the current is $2x_0$. The x and t coordinates may be rescaled and provided that the transformation obeys $t \sim x^2$, the governing equation (8) is unchanged. Hence, different values of x_0 correspond to different timescales. Therefore, without loss of generality, we use $x_0 = 1$ in the figures in this paper.

Equation (8) is parabolic and can be integrated numerically using a finite-difference scheme. We discretize the spatial coordinate using central differences. A MATLAB ODE solver is used for the time integration. The numerical results in the case of a uniform aquifer ($\Delta k = 0$) with no trapping ($\varepsilon = 0$) are shown in figure 2. The CO_2 is much less viscous than the ambient brine and we take the viscosity ratio to be $m = 0.2$. Figure 2 identifies that the CO_2 eventually detaches from the lower boundary. At early times, the CO_2 current spans the thickness of the aquifer with $h \sim 1$. This is known as 'confined' behaviour. At later times, the current slumps and occupies a thin region near the top boundary. The motion of the ambient fluid becomes unimportant. The current is then effectively 'unconfined' because the lower boundary has a negligible effect on the flow. We study these two regimes in turn and in both cases we quantify the influence of vertical permeability variations on the evolution. Throughout, we are particularly interested in the location of the leading contact point of the current, $x = x_f(t)$, where the interface touches the upper boundary. The extent of the current is an important quantity for determining the risk of leakage in the post-injection period and for determining the storage efficiency.

Confined behaviour

Equation (8) with initial condition (12) is self-similar at early times with

$$h = h(\xi), \qquad \xi = (x - x_0)/t^{1/2}. \qquad (13)$$

The current thickness, $h(\xi)$, satisfies the following equation

$$-\frac{1}{2}\xi\frac{\mathrm{d}h}{\mathrm{d}\xi} = \sigma\frac{\mathrm{d}}{\mathrm{d}\xi}\left[g(h)\frac{\mathrm{d}h}{\mathrm{d}\xi}\right]. \tag{14}$$

We obtain the boundary conditions at the leading and trailing contact points, $\xi_f > 0$ and $\xi_b < 0$, by considering the behaviour of equation (14) near $h = 0$ and $h = 1$,

$$\frac{\mathrm{d}h}{\mathrm{d}\xi} = -\frac{\xi_f}{2(1-\varepsilon)k(0)}, \quad h = 0, \quad \text{at} \quad \xi = \xi_f, \tag{15}$$

$$\frac{\mathrm{d}h}{\mathrm{d}\xi} = \frac{\xi_b}{2mk(1)}, \quad h = 1, \quad \text{at} \quad \xi = \xi_b. \tag{16}$$

Since $\partial h/\partial t = -\xi/(2t)\mathrm{d}h/\mathrm{d}\xi$ and $\mathrm{d}h/\mathrm{d}\xi < 0$, the current advances in $\xi > 0$ and recedes in $\xi < 0$, which determines the dependency of σ on ξ in equation (14). The system (14) with boundary conditions (15) and (16) is solved by numerically integrating inwards from the two boundaries, ξ_f and ξ_b, to $\xi = 0$. The unknown constants, ξ_f and ξ_b, are obtained by iterating and matching h and its first derivative at $\xi = 0$ (the first derivative is continuous because the flux is continuous everywhere). The interface shapes, obtained from equation (14), for three values of the trapping fraction, ε, are shown in figure 3 for an aquifer with constant permeability ($\Delta k = 0$) in the case that $m = 0.2$. Figure 4 shows the effect of different permeability structures on the interface shape. The similarity solution obtained here is an exact solution to the full governing equation (8) until the current detaches from the lower boundary.

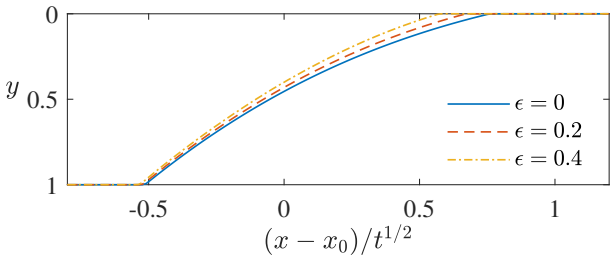

Figure 3. The confined early-time interface shapes in an aquifer with constant permeability ($\Delta k = 0$) in similarity coordinates, obtained from equation (14). Interface shapes are shown for three values of the trapping fraction, ε. The viscosity ratio is $m = 0.2$.

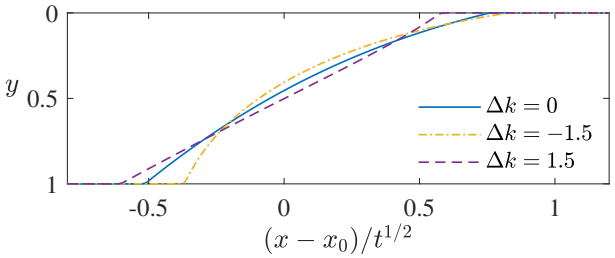

Figure 4. The shape of the confined current in similarity coordinates in the case that there is no trapping ($\varepsilon = 0$) and $m = 0.2$. Curves are shown for an aquifer with constant permeability ($\Delta k = 0$), with permeability that increases linearly towards the top ($\Delta k = -1.5$) and with permeability that decreases linearly towards the top ($\Delta k = 1.5$).

The location of the contact point at $h = 0$ in similarity coordinates, $\xi = \xi_f = (x_f - x_0)/t^{1/2}$, is shown in figure 5 for a range of linear permeability profiles and values of the trapping fraction, ε. In the case that the permeability increases towards the top of the aquifer ($\Delta k < 0$), the current has a greater extent at early times and vice versa for $\Delta k > 0$. This is because the flow speed increases towards the upper boundary when the permeability increases there. A larger trapping fraction, ε, reduces the extent of the current because the flux is reduced owing to the capillary trapping at the receding edge.

The current detaches from the lower boundary when the receding tips collide at $x = 0$, which corresponds to the time, $t = (x_0/\xi_b)^2$. Subsequently, the present analysis does not apply. There is a transition as the current slumps towards the upper boundary (see figure 2). Eventually the current occupies a thin region near the upper boundary, which is discussed next.

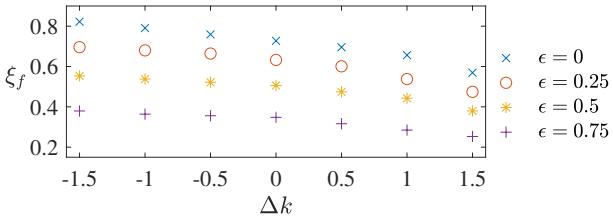

Figure 5. Location of the leading contact point, $\xi_f = (x_f - x_0)/t^{1/2}$, for the early-time confined self-similar behaviour with $m = 0.2$.

Unconfined behaviour

At late times, having slumped upwards away from the lower boundary, the CO_2 occupies a thin region beneath the upper boundary and $h \ll 1$. In this late-time, unconfined regime, the governing equation (8) reduces to

$$\frac{\partial h}{\partial t} = \sigma k(0)\frac{\partial}{\partial x}\left(h\frac{\partial h}{\partial x}\right). \tag{17}$$

The influence of the ambient fluid on the motion of the carbon dioxide is neglected. The permeability appears in equation (17) only through the value it takes at the top of the aquifer, $k(0)$. In the regime, $h \ll 1$, the current evolves as if in a uniform and unconfined aquifer. This problem has been well-studied and we outline the solution below.

For the case in which there is no trapping ($\varepsilon = 0$), equation (17) admits the following similarity solution [1]

$$h = \frac{t^{-1/3}}{6k(0)}\left\{\left[9k(0)x_0\right]^{2/3} - x^2/t^{2/3}\right\}, \tag{18}$$

where the dimensionless volume of the current is a constant, $2x_0$.

The evolution of the leading contact point, x_f is shown in figure 6 in the case that $\varepsilon = 0$. At early times, the position satisfies $x_f - x_0 \sim t^{1/2}$ (red dotted line) as discussed in the previous section. At late times, $x_f \sim t^{1/3}$ (red dashed line).

In the case that $\varepsilon \neq 0$, the late-time unconfined similarity scalings cannot be determined by dimensional analysis alone. Instead, equation (17) admits a self-similar solution of the second kind for which the exponents are determined from a nonlinear eigenvalue problem (for further details of this idea, see chapter 3 of [1]). The form of equation (17) suggests the following substitutions [6, 3]

$$x = c_1 k(0)^{1/3}\eta t^a, \tag{19}$$

$$h = c_2 k(0)^{-1/3} t^{2a-1}\Phi(\eta), \tag{20}$$

where the exponent a, which is to be determined, depends on ε whilst the constants c_1 and c_2 depend on the early-time behaviour. For details on determining a numerically, see [2]. We note that $a \leq 1/3$ with equality when $\varepsilon = 0$.

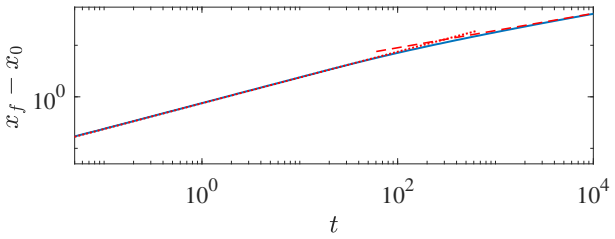

Figure 6. Location of the leading contact point, x_f, in an aquifer with constant permeability ($\Delta k = 0$), zero trapping ($\varepsilon = 0$) and a viscosity ratio of $m = 0.2$. The early confined behaviour is given by $x_f - x_0 \sim t^{1/2}$ (red dotted line). At late times, the position is given by $x_f \sim t^{1/3}$ (red dashed line).

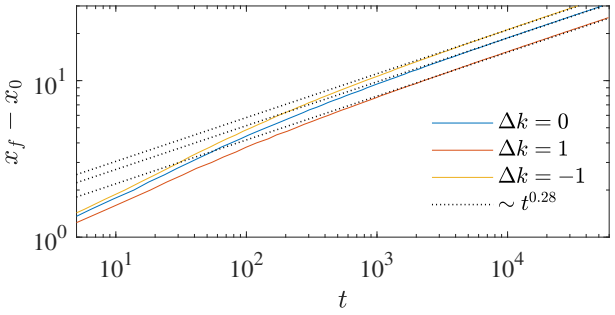

Figure 7. Locations of the leading contact point, x_f at late times in the case of an aquifer with constant permeability ($\Delta k = 0$), with permeability decreasing towards the top ($\Delta k = 1$) and with permeability increasing towards the top ($\Delta k = -1$). We use $\varepsilon = 0.6$ and $m = 0.2$. The second kind similarity scalings with $a = 0.28$ for $\varepsilon = 0.6$ are included.

Figure 7 shows the position of the leading contact point, x_f, relative to its initial position, x_0 at late times for three linear permeability profiles. The current runs much further in the case that the permeability increases towards the top boundary, as expected. The form of equation (17) and the solution (19) suggest that the extent is varied by a factor $k(0)^{1/3}$ and the height by a factor $k(0)^{-1/3}$. In figure 8, the interface shapes corresponding to figure 7 are shown at $t = 10^4$ in rescaled coordinates. The shapes are not quite identical because they have a slight dependency on the early-time behaviour, which is sensitive to the permeability structure. This sensitivity can be observed by considering aquifers with equal permeability at the top boundary rather than aquifers with the same mean permeability. Figure 9 shows the front locations for two different permeability structures but with the same permeability at the top. The increased extent tends to a constant at late times because the late-time behaviour depends only on the permeability at the top. The extent is greater in a uniform aquifer than an aquifer with permeability decreasing towards the bottom ($\Delta k = -1$) because the inward tip on the lower boundary propagates slower when the permeability is low there and so more CO_2 is trapped away from the lower boundary.

Conclusion

We have shown that the run-out extent of the CO_2 is increased in the case of higher permeability at the top of the aquifer. The extent is primarily controlled by the permeability there rather than the mean permeability or the permeability structure in the rest of the aquifer because at late times, the current occupies a thin region near the upper boundary. The early-time behaviour, which is sensitive to the permeability structure has only a second-order effect on the run-out extent because it determines the relatively

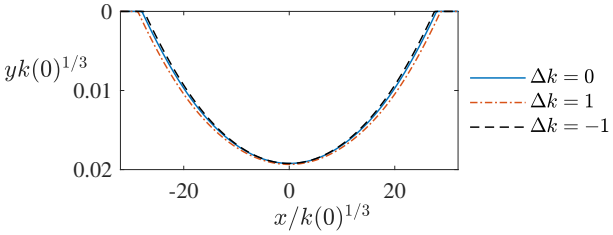

Figure 8. The interface shapes corresponding to figure 7 at $t = 10^4$ in rescaled coordinates.

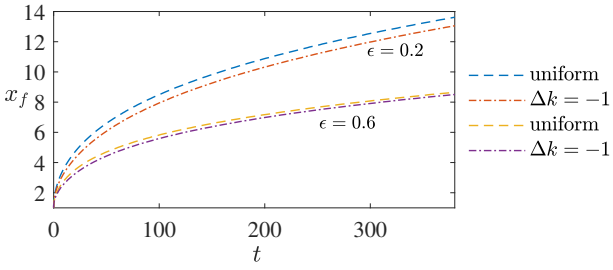

Figure 9. Locations of the leading contact point, x_f, in aquifers with the same permeability at the top boundary for two values of ε.

small volume of CO_2 that is stored away from the top boundary. This suggests that modelling aquifers as vertically uniform with permeability equal to the permeability at the top boundary is a reasonable approximation for quantifying runout distances.

References

[1] Barenblatt, G. I. (1996). Scaling, self-similarity, and intermediate asymptotics: dimensional analysis and intermediate asymptotics. *Cambridge University Press*.

[2] Bear, J. and Ryzhik, V. (1998). On the displacement of NAPL lenses and plumes in a phreatic aquifer. *Transport in porous media*, 33(3), 227–255. (DOI:10.1023/A:1006544629038).

[3] Hesse, M. A. and Orr Jr, F. M. and Tchelepi, H. A. (2008). Gravity currents with residual trapping. *Journal of Fluid Mechanics*, 611, 35–60 (DOI:10.1017/S002211200800219X).

[4] Hinton, E. M. and Woods, A. W. (2018). Buoyancy-driven flow in a confined aquifer with a vertical gradient of permeability. *Journal of Fluid Mechanics*, 848, 411–429 (DOI:10.1017/jfm.2018.375).

[5] Hinton, E. M. and Woods, A. W. (2019). The effect of vertically varying permeability on tracer dispersion. *Journal of Fluid Mechanics*, 860, 384–407 (DOI:10.1017/jfm.2018.891).

[6] Kochina, I. N. and Mikhailov, N. N. and Filinov, M. V. (1983). Groundwater mound damping. *International Journal of Engineering Science*, 21(4), 413–421 (DOI:10.1016/0020-7225(83)90124-6).

[7] MacMinn, C. W. and Juanes, R. (2009). Post-injection spreading and trapping of CO_2 in saline aquifers: impact of the plume shape at the end of injection. *Computational Geosciences*, 13(4) 483–491 (DOI:10.1007/s10596-009-9147-9).